

# Synthesis of 1D Polymer/Zeolite Nanocomposites under High Pressure

Mario Santoro,<sup>\*,†,‡</sup> Demetrio Scelta,<sup>‡,§</sup> Kamil Dziubek,<sup>‡,||</sup> Matteo Ceppatelli,<sup>§,‡</sup> Federico A. Gorelli,<sup>†,‡</sup> Roberto Bini,<sup>‡,⊥</sup> Gaston Garbarino,<sup>#</sup> Jean-Marc Thibaud,<sup>∇</sup> Francesco Di Renzo,<sup>∇</sup> Olivier Cambon,<sup>∇</sup> Patrick Hermet,<sup>∇</sup> Jerome Rouquette,<sup>∇</sup> Arie van der Lee,<sup>¶</sup> and Julien Haines<sup>∇</sup>

<sup>†</sup>Istituto Nazionale di Ottica, CNR-INO, 50019 Sesto Fiorentino, Italy

<sup>‡</sup>European Laboratory for non Linear Spectroscopy (LENS), 50019 Sesto Fiorentino, Italy

<sup>§</sup>Istituto di Chimica dei Composti Organo-Metallici, CNR-ICCOM, 50019 Sesto Fiorentino, Italy

<sup>||</sup>Faculty of Chemistry, Adam Mickiewicz University, Umultowska 89b, 61-614 Poznań, Poland

<sup>⊥</sup>Dipartimento di Chimica, Università degli Studi di Firenze, 50019 Sesto Fiorentino, Italy

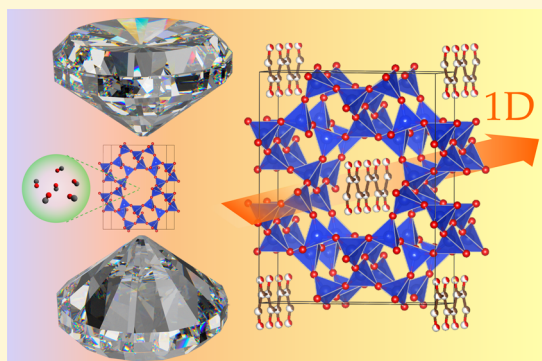
<sup>#</sup>European Synchrotron Radiation Facility, 38343 Grenoble, France

<sup>∇</sup>Institut Charles Gerhardt Montpellier, UMR 5253 CNRS-Université de Montpellier-ENSCM, 34095 Montpellier, Cedex 5, France

<sup>¶</sup>Institut Européen des Membranes de Montpellier, UMR 5635 CNRS-ENSCM-Université de Montpellier, 34095 Montpellier, Cedex 5, France

## Supporting Information

**ABSTRACT:** Recently, simple carbon based polymers have been synthesized at high pressures in silicalite, a pure SiO<sub>2</sub> zeolite with a 3D system of mutually interconnected microchannels. These protocols permitted otherwise unstable polymers to be stabilized and protected from the atmosphere and to obtain an entirely novel class of nanocomposites with modified physical properties. In these 3-D systems, channel interconnection may prevent ideal, isolated polymer chains to be obtained. In this work, the high pressure (5–10 GPa) synthesis of two archetypal, linear polymers polyacetylene (PA) and polycarbonyl (pCO) in the 1D channel system of the pure SiO<sub>2</sub> zeolite ZSM-22 (TON) has been performed. The two resulting nanocomposites PA/TON and pCO/TON are organic/inorganic composite materials, which are good candidates as highly directional semiconductors and high energy density materials, respectively. The synthesis was performed in diamond anvil cells, starting from dense C<sub>2</sub>H<sub>2</sub> and CO, confined in ZSM-22, and the nanocomposites were recovered at ambient conditions. The monomer polymerization was proven by IR spectroscopy and synchrotron X-ray diffraction measurements. DFT calculations were performed in order to obtain insight about the configurations of the 1D embedded polymers.



## INTRODUCTION

High pressure (HP) conditions, in the range of tenths/hundreds of GPa, lead to development of new physics, chemistry and materials science with the discovery of novel phases and materials.<sup>1–12</sup> One remarkable case in this respect is the purely pressure induced self-assembling/polymerization of simple, carbon bearing molecules such as acetylene, ethylene, and carbon monoxide, obtained in the GPa range.<sup>13–15,11,16–25</sup> These fundamental studies also have potential implications for technology. Polyethylene (PE) is the most widely used plastic material; polyacetylene (PA) is a textbook model, conductive polymer, and polycarbonyl (pCO) is a good candidate as a high energy storage material with an energy density comparable with that of dynamite. HP polymerization avoids the polluting use of catalysts and radical initiators. Unfortunately, while HP polymerization of C<sub>2</sub>H<sub>4</sub> leads to crystalline polymers with

ultrahigh molecular weight,<sup>11</sup> polymerization of C<sub>2</sub>H<sub>2</sub> and CO ends in final products which are structurally and chemically disordered that certainly limits potential technological applications. Poly-C<sub>2</sub>H<sub>2</sub> (PA) obtained at high pressures is not only made of conjugated (C<sub>2</sub>H<sub>2</sub>)<sub>n</sub> chains with C in sp<sup>2</sup> hybridization as the chains are also highly branched and contain terminations via sp<sup>3</sup> C sites.<sup>13</sup> Poly-CO, on the other hand, is an entirely random 3D polymer made of a large variety of functional groups such as carbonyls, particularly in the form of anhydride moieties, epoxy rings, and C–C–O and C–O–C groups with also an excess of molecular CO<sub>2</sub>; in addition, both

Received: April 26, 2016

Revised: May 19, 2016

Published: May 22, 2016

PA and pCO are strongly damaged by exposure to light and/or moisture.<sup>17–25</sup>

Recently, significant effort has been made in polymerizing  $C_2H_4$ ,<sup>26</sup>  $C_2H_2$ ,<sup>27</sup> and  $CO$ <sup>28</sup> at high pressures, under strong confinement inside the pore system of zeolites. The aim of this research is at least threefold: (i) unveiling fundamental aspects on self-assembling of dense matter in a strongly confined space and with reduced dimensionality, (ii) synthesizing organic polymers in chemically protecting, inorganic scaffolds, and (iii) synthesizing entirely novel nanocomposite materials with modified physical and chemical properties with respect to the two components, the polymer and the zeolite. These protocols only use pressure as the driving force (and also UV light in the case of ethylene) with no catalysts and/or radical initiators. Indeed, PE, PA, and pCO have been synthesized in the GPa range in the microchannels of silicalite (SIL), an electrically neutral, noncatalytic, hydrophobic, all  $SiO_2$  zeolite. Silicalite is characterized by a framework of 4-, 5-, 6-, and 10-membered rings of corner-sharing  $SiO_4$  tetrahedra forming interconnected, mutually orthogonal straight and sinusoidal 5.5 Å diameter channels.<sup>29,30</sup> Single PE, PA, and pCO polymeric chains are efficiently formed both in straight and in sinusoidal channels, leading to nanocomposite materials that were termed PESIL, PASIL, and pCOSIL, respectively. Indeed, total chemical order and some degree of structural order were obtained in the case of CO, where all-transoid polycarbonlyl  $[-(C=O)-]_n$  was formed in the channels of silicalite. Interestingly, a bulk solid phase of this type of polymer was predicted to form from CO at high pressures and to be stable/metastable in a large range of pressures, including ambient conditions,<sup>31</sup> but this polymer has not been synthesized so far. Strong confinement of self-assembling, monomeric CO in the channels of zeolites at high pressure seems to be a unique way, maybe the only way, to obtain chemically ordered  $[-(C=O)-]_n$  chains. Unfortunately, the PE, PA, and pCO/silicalite nanocomposites are affected by at least two drawbacks, which may limit their ideal physical properties, such as conductivity for PA and, as a consequence, potential applications of these materials. First, sinusoidal polymeric chains assembled in the sinusoidal channels are highly strained as these polymers are linear in the unstrained form. Also, as verified for PASIL, cross-linking of linear and sinusoidal channels may lead to branching of confined polymeric chains. In this work, we aim to overcome these limitations, which could permit the exploitation of the directional properties of the polymers, by using a noncatalytic, all  $SiO_2$  zeolite, ZSM-22 (TON),<sup>32</sup> with a 1D channel system as the host material. The unidirectional channels of TON have elliptical cross sections of 5.7 and 4.6 Å axes, respectively, which may also be useful in driving the planar assemblage of the carbon backbone of the polymeric chains. In the following, we present the high pressure synthesis and spectroscopic and structural characterization of PA/TON and pCO/TON composites, where indeed 1D PA and pCO are formed in the host channels of TON.

## ■ EXPERIMENTAL AND COMPUTATIONAL METHODS

The TON zeolite was prepared by sol–gel techniques using triethylenetetramine as the structure directing agent followed by crystallization at 170 °C under hydrothermal conditions as described previously.<sup>32</sup> The sample was calcined in air at 550 °C to remove the organic template. Membrane diamond anvil cells (MDAC) equipped with stainless steel gaskets were used for the polymerization of

confined acetylene and CO in TON, i.e., for the synthesis of PA/TON and pCO/TON. Typical sample dimensions were 100–300 μm in diameter and 40–50 μm in thickness. Acetylene (purity 99.6% from Rivoira and further purified by us<sup>13</sup>) was loaded cryogenically at 190 K together with hydrophobic TON powder. Gaseous acetylene was allowed to flow at ambient pressure through the cooled sample chamber where it froze all around and inside the pores of the zeolite, and external pressure was then applied, similarly to the loading of pure acetylene.<sup>13</sup> In contrast, carbon monoxide (purity 99.99% from Sapio) was loaded cryogenically in the liquid phase, at 1–2 bar and 77 K, together with the TON powder. A ruby chip was also put in the sample chambers for pressure measurements.<sup>33</sup> Good mechanical matching between TON and monomers guarantees that pressure is efficiently transmitted from the zeolite matrix to the embedded monomers and, consequently, that TON and these monomers are really compressed together. Mechanical matching is due to empty TON and pure solid molecular systems having reasonably similar compressibility, slightly lower than one tenth of  $GPa^{-1}$  for TON and equal to a few tenths of  $GPa^{-1}$  for the molecular substances. On the other hand, the slightly higher compressibility of the dense monomers is responsible for these substances being efficiently packed into the zeolites matrix under pressure before the framework collapse, which in turn deactivates pressure induced amorphization, at least in the range of pressures where polymerization is observed in this work.<sup>34</sup>

IR absorption spectra were measured by a Bruker IFS-120 HR Fourier transform infrared spectrometer equipped with a global lamp, a KBr beam splitter, an MCT detector, and an optical beam condenser based on ellipsoidal mirrors (ref 35 and references therein). The spectral resolution was 1  $cm^{-1}$ . Some synchrotron FTIR measurements on PA/TON were also performed at the AILES and SSSI beamlines at SOLEIL and ELETTRA, respectively. Synchrotron IR data are consistent with those obtained from the laboratory setup and are not reported here. Micro-Raman measurements were also attempted using the 647.1 nm line of a  $Kr^+$  laser, but results were severely limited by fluorescence emission and, in the case of pCO/TON, by photodegradation of samples. Angle dispersive, powder X-ray diffraction (XRD) patterns were measured by using both a laboratory source and a synchrotron facility. Synchrotron XRD were measured at the ID09A beamline of the ESRF, with a monochromatic beam ( $\lambda = 0.414132$  Å for pCO/TON and  $\lambda = 0.415352$  Å for PA/TON) and a MAR555 flat panel detector. The nominal size of the focal spot was 20 μm. The diffraction patterns were analyzed and integrated using the FIT2D program.<sup>36</sup> The Rietveld refinements were performed with the program Fullprof.<sup>37</sup> Fourier maps were calculated using the program GFOURIER.<sup>38</sup>

Density functional theory (DFT) based calculations were performed on the cis-PA/TON and the trans-PA/TON as models of the ordered state of the PA/TON. Similarly, the cisoid-pCO/TON and the transoid-pCO/TON were used as models of the pCO/TON. We used the SIESTA package<sup>39</sup> and the generalized gradient approximation to the exchange correlation functional as proposed by Perdew, Burke, and Ernzerhof.<sup>40</sup> Core electrons were replaced by nonlocal norm-conserving pseudopotentials. The valence electrons were described by a double- $\zeta$  singly polarized basis set. The localization of the basis is controlled by an energy shift of 50 meV. Real space integration was performed on a regular grid corresponding to a plane-wave cutoff around 300 Ry. Atomic positions were relaxed at the experimental lattice parameters using a conjugate gradient until the maximum residual atomic force was smaller than 0.008 eV/Å. These relaxations were performed using a  $6 \times 6 \times 4$ ,  $6 \times 6 \times 4$ ,  $8 \times 8 \times 8$ , and  $4 \times 4 \times 6$  k-point mesh for the cis-PA/TON, trans-PA/TON, cisoid-pCO/TON, and transoid-pCO/TON, respectively. Electronic density-of-states of these four ordered models have been calculated using a  $25 \times 25 \times 20$  k-point mesh. We found that the cis-PA/TON and transoid-pCO/TON are semiconducting whereas the trans-PA/TON and cisoid-pCO/TON are metallic. Zone-center phonons of cis-PA/TON and trans-PA/TON were calculated within the harmonic approximation by finite difference of the Hellmann–Feynman forces with an atomic displacement of 0.03 Å and using the same k-point mesh considered for the relaxation. Positive and negative displace-

ments are used to minimize the anharmonic effects. For the all-transoid CO polymer, we used 50 k-points along the polymer direction, and a vacuum size of 12 Å was used to avoid interchain interactions in the two other directions.

## RESULTS AND DISCUSSION

**IR Characterization of PA/TON and pCO/TON.** IR absorption spectroscopy, which is a powerful technique for determining chemical species, was used for tracking the time evolution of pressure induced polymerization of C<sub>2</sub>H<sub>2</sub> and CO in TON and to characterize the final, nanocomposite material. Similarly to polymerization in bulk C<sub>2</sub>H<sub>2</sub> and CO and of the same molecules confined in silicalite, polymerization in TON was complete in a few hours/days, at about 5 GPa for C<sub>2</sub>H<sub>2</sub> and 7–10 GPa for CO, respectively.<sup>13,25,27,28</sup> The fact that polymerization occurs at similar pressures in bulk and in the embedded monomers suggests that indeed pressure is the major driving force for the self-assembly of the monomers in the channels of TON and that the potential catalytic role of any OH impurities at the inner pore surface is rather negligible. Figure 1 shows the selected spectral region of C–H stretching

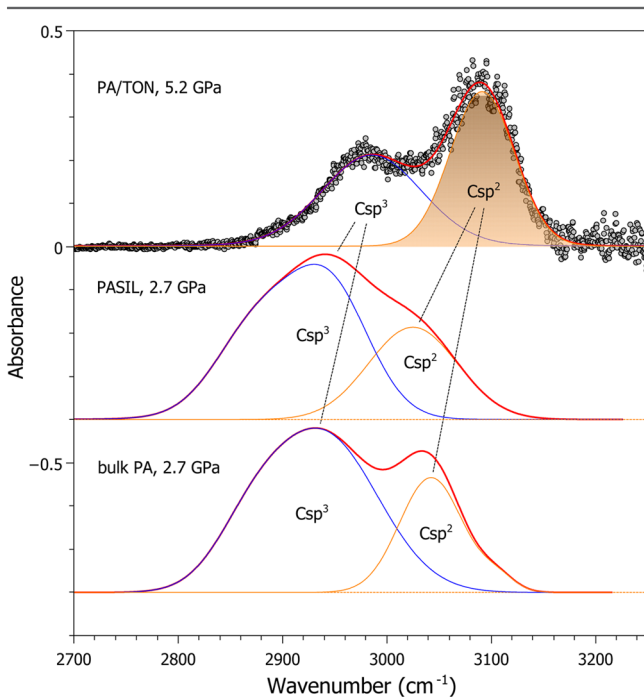


**Figure 1.** IR absorption spectrum of PA/TON (top), in the selected frequency range of the C–H stretching modes, at 5.2 GPa. Conjugated chains of PA are identified by the C(sp<sup>2</sup>)-H peak (orange, with full area), whereas the C(sp<sup>3</sup>) peak (blue) reveals branching and terminations of the chains, most likely related to the surrounding bulk polymer. Reproduced spectra of PASIL and bulk PA are also reported for comparison.<sup>27</sup> Absorbances of the three spectra were normalized to the same peak intensity. Spectra are vertically shifted by a constant, for the sake of visual clarity.

modes of PA in the PA/TON composite, at high pressures, along with similar literature spectra for bulk PA and PASIL, which are reported for comparison.<sup>27</sup> Peaks assigned to modes of CH groups with C in sp<sup>2</sup> and sp<sup>3</sup> hybridization are indicated; these peaks correspond to PA chains/oligomers and points of branching and termination of the chains, respectively. Therefore, the ratio  $r$  between the integrated absorbance of sp<sup>2</sup> and sp<sup>3</sup> peaks is a quality parameter, indicating the degree of

deviation from the ideal, all conjugated chain of PA. In perfect PA  $r$  would be infinite. Indeed, in bulk PA, PASIL, and PA/TON  $r$  is equal to 0.35, 0.46, and 1.1, respectively, which, once the different absorption cross sections for sp<sup>2</sup> and sp<sup>3</sup> C sites are taken into account,<sup>41</sup> leads to sp<sup>2</sup>/sp<sup>3</sup> ratios of 0.52 (bulk PA), 0.67 (PASIL), and 1.5 (PA/TON). Actually, the real sp<sup>2</sup>/sp<sup>3</sup> ratio in PA/TON is expected to be even higher than 1.5, since the powdered nanocomposite is surrounded by bulk PA, which may be the main source of the C(sp<sup>3</sup>)-H stretching IR peak. In the end, the result is that while the degree of branching in PA assembled in PASIL is comparable to that of bulk PA, due to the non-1D and interconnected character of the host channels in silicalite, the 1D channels of TON indeed drive the formation of virtually nonbranched PA chains, which is of paramount importance for potential applications. In a similar manner, Figure 2 shows the IR spectrum at ambient conditions

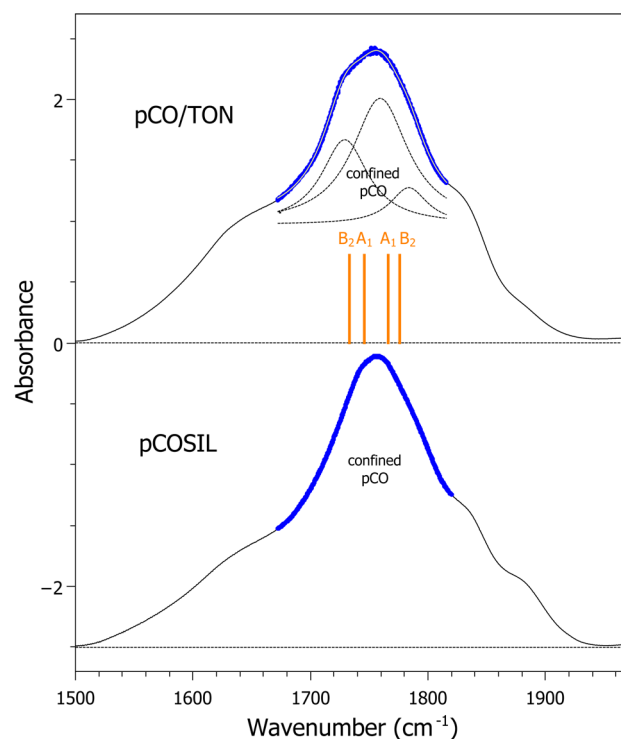


**Figure 2.** IR absorption spectrum of pCO/TON (top), in the selected C=O stretching frequency region. The sample was recovered in the gasket, taken out of DAC, and exposed to atmosphere. The peak assigned to confined pCO in host TON is schematically marked by the blue color. Three Lorentzian peaks (dashed lines for each and continuous yellow line for the sum of the three) have been fitted to this peak. Vertical bars: DFT calculated frequencies for cisoid-pCO/TON. Spectrum of pCOSIL is also reported for comparison.<sup>28</sup> Absorbances of the two spectra were normalized to the same peak intensity. Spectra are vertically shifted by a constant, for the sake of visual clarity.

of pCO/TON in a free-standing gasket, which was taken out of the DAC and exposed to the atmosphere, together with a literature spectrum of pCOSIL. We limit our discussion to the C=O stretching region (1500–2000 cm<sup>-1</sup>) and only for recovered samples outside of the DACs, since saturating peaks of TON dominate other spectral regions at lower frequencies and because the strong two-phonon peak of diamond partially overlaps with the C=O stretching peak of the nanocomposites. We see that the C=O complex band is made of a sharper,

central peak, marked by the blue color, which also exhibits a fine structure and is superimposed on a much broader one. Following the discussion on pCOSIL,<sup>28</sup> the sharper peak arises from confined pCO, whereas the broader one is mainly due to bulk pCO which surrounds the powdered pCO/TON and, to a much less degree, by weak peaks of TON. The broad band of bulk pCO is most likely to be related to different kinds of carbonyl groups in this chemically disordered material. Instead, the sharper peak of confined pCO is a strong sign of chemical order of this polymer in pCO/TON. Indeed, the ideal, infinite all-transoid  $[-(C=O)-]_n$  chain has only one IR C=O stretching active mode, which is compatible with the single peak of confined pCO in pCOSIL. On the other hand, the corresponding peak in pCO/TON is split in three components by about 25–30  $\text{cm}^{-1}$ . The splitting indicates a more complex structure or a stronger interaction with the host zeolite than in the case of “isolated” all-transoid polycarbonyl (transoid-pCO), which in addition is not compatible with the symmetry of the unit cell of the host TON zeolite. The most simple symmetry-compatible configuration is that with alternating cisoid and transoid (C=O) conformations, termed cisoid-pCO/TON.

DFT calculations on transoid-pCO/TON predict eight infrared A-modes [1606, 1607, 1643, 1656, 1665, 1684, 1690, and 1692  $\text{cm}^{-1}$ ] in this region whereas calculations on cisoid-pCO/TON give four infrared modes [1776 (B2), 1766 (A1), 1746 (A1), and 1733  $\text{cm}^{-1}$  (B2)]. This latter configuration of the pCO is therefore in much better agreement with the experimental spectrum considering the number of predicted modes and their frequencies. Further discussion of this aspect follows in the XRD section, where results of structural refinement are presented.

**Determination and Refinement of the Structures of PA/TON and pCO/TON by XRD.** Laboratory XRD has been used to qualitatively check the degree of pore filling of TON with acetylene/PA and CO/pCO during the synthesis of the composite materials, at high pressures. However, the limited data quality of laboratory XRD and particularly the low signal-to-noise ratio and low angular resolution prevented quantitative structure refinements of PA/TON and pCO/TON. Synchrotron powder XRD measurements were thus performed on the nanocomposite materials, which were recovered in the gasket at ambient pressure. Very high quality data were obtained for PA/TON. Preliminary refinements were performed using the empty  $\text{SiO}_2$  framework based on the structural model of Marler.<sup>42</sup> The fit was very poor with a Bragg  $R$ -factor of 30.1%. A Fourier difference map was then calculated, which enabled 4 sites for carbon atoms per unit cell to be located. These four sites, each with a multiplicity of 4, lying in the  $yz$  plane cannot all be occupied simultaneously as the C–C distances would be too short. The refinement with the 24  $\text{SiO}_2$  formula units from the framework and the 16 C atoms in the pores with the chemical site occupancy fixed to 50% gave a very good fit with a Bragg  $R$ -factor of 4.2%, Figure 3 (top), Table 1, and Table 1SI. The improvement in the fit obtained by including 16 C atoms with 50% occupancy is consistent with the presence of a degree of disorder in the chain isomers and positions, which is in better agreement with the residual electron density in the center of the pores in the observed Fourier map, Figure 4 (top), than a model with 8 C atoms fully occupying their crystallographic sites. The PA content is thus four chains per unit cell and consequently one chain per pore corresponding to 100% pore filling. In order to obtain further information on the nature of the PA chains inside the pores, a second refinement

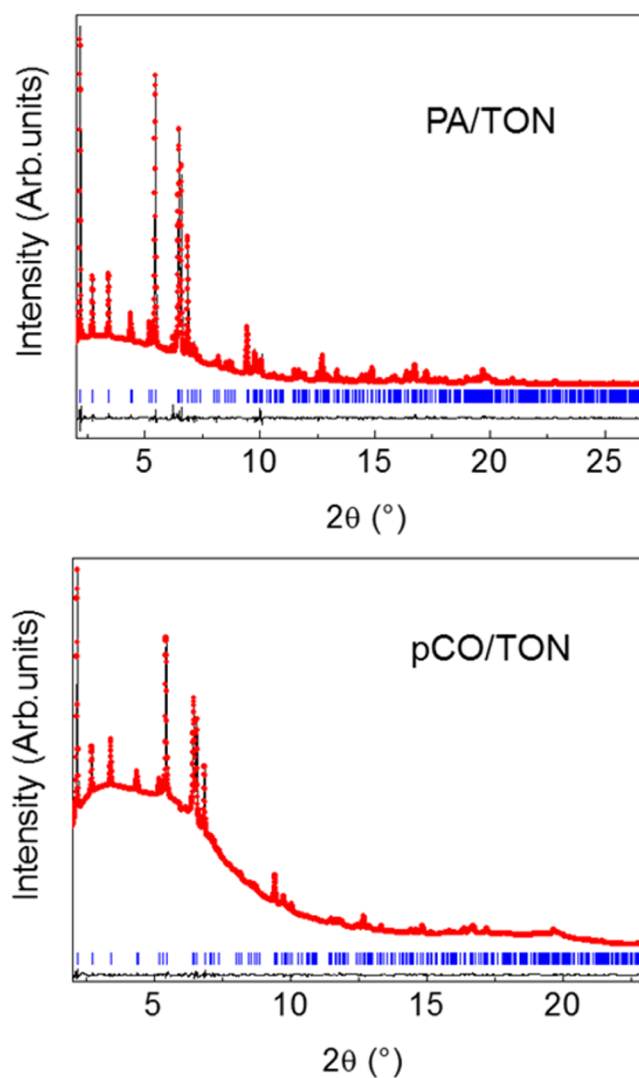


**Figure 3.** Experimental (dots) and calculated (solid line) XRD profiles from the Rietveld refinement of PA/TON (top) and pCO/TON (bottom) at ambient pressure; the samples were recovered in the gasket. The difference profile is on the same scale. Vertical bars indicate the positions of the calculated Bragg reflections.

**Table 1. Structural Data and Agreement Factors Obtained from Rietveld Refinements for PA/TON and pCO/TON (space group  $Cmc2_1$ ,  $Z = 8$ )<sup>a</sup>**

cell parameters	PA/TON	pCO/TON
$a$ (Å)	13.8553(1)	13.8867(4)
$b$ (Å)	17.3992(2)	17.4430(9)
$c$ (Å)	5.03855(5)	5.0475(2)
$V$ (Å <sup>3</sup> )	1214.64(2)	1222.63(8)
$R_p$ (%)	10.2 [11.9]	9.1 [9.8]
$R_{wp}$ (%)	9.4 [10.7]	5.7 [6.3]
$R_{Bragg}$ (%)	4.2 [5.7]	3.1 [3.2]

<sup>a</sup>Agreement values with the atoms of the embedded polymers fixed to the values obtained from the relaxed DFT structures with fixed cell parameters are given in square brackets. The full list of structural data is in the Supporting Information (Table 1SI and 2SI).

was performed using the relaxed cis-PA chain from the DFT calculations with fixed positions, Table 1, Table 2SI, and Figure 5 (top). We can again note that DFT calculations also confirm

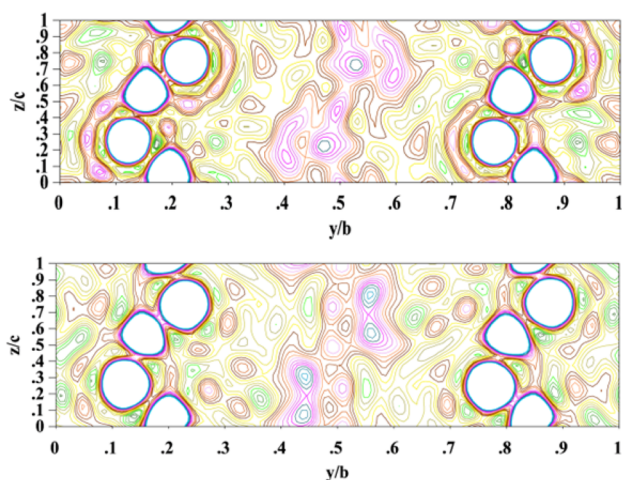


**Figure 4.** Section of the electron density map at  $x/a = 0.5$ , obtained by Fourier inversion of observed structure factor amplitudes and model phases (the isocontour interval is  $0.1 \text{ e}/\text{\AA}^3$ ). The white circles at  $y/b = 0.1-0.25$  and  $y/b = 0.75-0.9$  represent the framework atoms, whereas the polymerized chains are visible at  $y/b = 0.4-0.6$  for PA/TON (top) and pCO/TON (bottom).

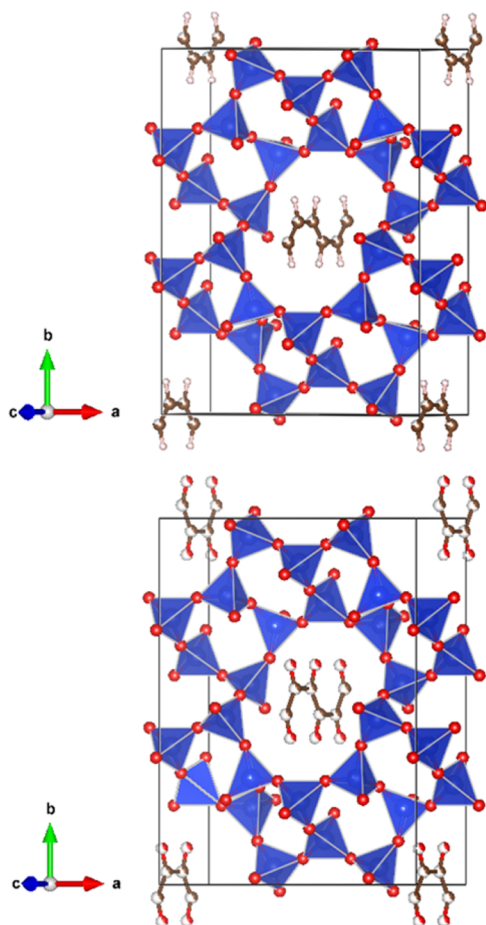


**Figure 5.** Structure of PA/TON (top) and pCO/TON (bottom).  $\text{SiO}_4$  tetrahedra are represented in blue. Black/white, white, and red/white spheres represent carbon, hydrogen, and oxygen atoms, respectively, from the relaxed structure of PA and pCO obtained from DFT calculations and fixed during the refinement.

that the PA chains have a planar zigzag conformation parallel to the  $bc$  plane. The Bragg  $R$ -factor increased to 5.7% indicating

that such a model, although it is much closer to the final model in terms of the quality of the fit than the empty pore model, does not completely reproduce the data. This result and the fact that the observed Fourier map contains additional features with respect to the four peaks along  $z$  in the center of the pores expected for the carbon atoms of pure *cis*-PA indicates that the true structure is disordered. It can be noted that an ordered *pure-trans* PA is not consistent with the symmetry of TON and such a structure would imply an increase in the size of the unit cell and a change in symmetry and consequently changes in the X-ray diffraction pattern, which is not observed in the experimental data.

A similar approach was adopted for the pCO/TON nanocomposite. Again the C and O atoms could be readily located on the Fourier difference map and incorporated in the structural model, although they could not be chemically distinguished because of their nearly equal scattering power. The fit obtained from the Rietveld refinement was very good with a Bragg  $R$ -factor of 3.1%, Figure 3 (bottom).

The refined occupations give a CO content of 2.4 molecules per unit cell corresponding to 30% pore filling in a statistical distribution. Incomplete pore filling is probably linked either to an incomplete polymerization of CO and subsequent loss of remaining monomers after pressure release or to incomplete filling by the initial CO monomers. The present structural model consists of alternating *cis* and *transoid* configurations, which are commensurate with the framework and consistent with the observed Fourier map, Figure 4 (bottom). This model gives unreasonable bond lengths and angles. As in the previous case, the relaxed chain from DFT calculations was used in a second refinement with fixed positions for the chain atoms, Figure 5 (bottom) and Table 1. In this case the Bragg  $R$ -factor was essentially identical to the first refinement, indicating that the refinement is not very sensitive to minor shifts in the positions of the guest atoms. The DFT model can thus correctly reproduce the experimental data, both on a structural level and on a vibrational level in the infrared spectrum.

In addition, DFT calculations of the electronic density-of-states of the ordered models of pCO/TON and PA/TON show van Hove singularities within the band gap of the TON due to the 1-D nature of the polymer chains. This result suggests that these singularities could be observed in the corresponding experimental samples, which is beyond the scope of the present study. An estimate of the band gap of these nanocomposites is presently not possible as we found that the ordered models of PA/TON can be metallic (*trans*-PA/TON) or semiconducting (*cis*-PA/TON). The same problem occurs for the ordered models in pCO/TON.

## CONCLUSIONS

We have developed high pressure technological protocols, in the GPa range, to synthesize novel organic/inorganic subnanocomposite materials made of 1D guest polymers, PA and pCO, within the driving 1D microchannels of an all  $\text{SiO}_2$  noncatalytic zeolite ZSM-22 (TON). Dense acetylene and CO were indeed inserted in TON, and purely pressure induced polymerization of the monomers was obtained, leading to two new materials: PA/TON and pCO/TON. Characterization by IR spectroscopy, synchrotron XRD, full structural refinements, and DFT simulations show that the guest polymers have a strict planar conformation, which is most likely due to the elliptical shape of the host channels, and that they are mainly in the *cis* configuration, although PA is affected by some degree of

disorder within the plane. Remarkably, confined pCO is chemically ordered in contrast to bulk pCO observed so far, which is structurally and chemically disordered. On a general ground, our protocols indicate new chemical routes for synthesizing composite materials, where an inorganic scaffold drives the formation of, supports, and protects from the atmosphere an embedded organic polymer with low dimensionality, which in turn leads to overall novel materials with important physicochemical properties. In the present case, pCO/TON is a material with an energy storage capacity comparable to or even higher than that of dynamite. The protecting TON truly allows this energy to be retained/stored in the presence of atmospheric moisture, whereas pure bulk pCO immediately releases the stored energy when exposed to the atmosphere after the high pressure synthesis. In the case of PA/TON, the zeolite is also a unique way to prevent PA from reacting with the atmospheric moisture. In addition, the 1D nature of the polymers, in particular the van Hove singularities predicted by DFT in the density of states of valence electrons, which are confined in the transverse directions and free or quasi-free in the long direction, leads to the potential use of this class of materials as quantum devices for important applications such as quantum computation.

## ■ ASSOCIATED CONTENT

### Supporting Information

The Supporting Information is available free of charge on the ACS Publications website at DOI: [10.1021/acs.chemmater.6b01639](https://doi.org/10.1021/acs.chemmater.6b01639).

Tables 1SI and 2SI, containing all refined structural data for PA/TON and pCO/TON (PDF)

Crystallographic Information File for PA/TON (CIF)

Crystallographic Information File for pCO/TON (CIF)

## ■ AUTHOR INFORMATION

### Corresponding Author

\*(M.S.) E-mail: [santoro@lens.unifi.it](mailto:santoro@lens.unifi.it).

### Notes

The authors declare no competing financial interest. Crystallographic Information Files (CIF) are also deposited in the Cambridge Structural Database (CCDC 1480714–1480715).

## ■ ACKNOWLEDGMENTS

We are grateful for the support from PICS bilateral project CNR/CNRS (Italy/France), 2014–2016: Multifunctional zeolite/polymer nanocomposites. We would like to thank the LabEx CheMISyst (ANR-10-LABX-05-01) for supporting the work performed in Montpellier. We also thank the Deep Carbon Observatory (DCO) initiative under the project *Physics and Chemistry of Carbon at Extreme Conditions* and the Ente Cassa di Risparmio di Firenze under the project Firenze Hydrolab 2. K.D. acknowledges the Polish Ministry of Science and Higher Education for financial support through the “Mobilność Plus” program.

## ■ REFERENCES

(1) Dalladay-Simpson, P.; Howie, R. T.; Gregoryanz, E. Evidence for a new phase of dense hydrogen above 325 gigapascals. *Nature* **2016**, *529*, 63–67.

(2) Drozdov, A. P.; Erements, M. I.; Troyan, I. A.; Ksenofontov, K.; Shylin, S. I. Conventional superconductivity at 203 K at high pressures in the sulfur hydride system. *Nature* **2015**, *525*, 73–77.

(3) Kim, D. Y.; Stefanoski, S.; Kurakevych, O. O.; Strobel, T. A. Synthesis of an open-framework allotrope of silicon. *Nat. Mater.* **2015**, *14*, 169–173.

(4) Santoro, M.; Gorelli, F. A.; Bini, R.; Salamat, A.; Garbarino, G.; Levelut, C.; Cambon, O.; Haines, J. Carbon enters silica forming a cristobalite-type CO<sub>2</sub>–SiO<sub>2</sub> solid solution. *Nat. Commun.* **2014**, *5*, 3761.

(5) Santoro, M.; Gorelli, F. A.; Haines, J.; Cambon, O.; Levelut, C.; Garbarino, G. Silicon carbonate phase formed from carbon dioxide and silica under pressure. *Proc. Natl. Acad. Sci. U. S. A.* **2011**, *108*, 7689–7692.

(6) Ma, Y.; Erements, M.; Oganov, A. R.; Xie, Y.; Trojan, I. A.; Medvedev, S.; Lyakhov, A. O.; Valle, M.; Prakapenka, V. Transparent dense sodium. *Nature* **2009**, *458*, 182–186.

(7) Ciabini, L.; Santoro, M.; Gorelli, F. A.; Bini, R.; Schettino, V.; Raugei, S. Triggering dynamics of the high-pressure benzene amorphization. *Nat. Mater.* **2007**, *6*, 39–43.

(8) Lundegaard, L. F.; Weck, G.; McMahon, M. I.; Desgreniers, S.; Loubeyre, P. Observation of an O<sub>8</sub> molecular lattice in the  $\epsilon$  phase of solid oxygen. *Nature* **2006**, *443*, 201–204.

(9) Santoro, M.; Gorelli, F. A.; Bini, R.; Ruocco, G.; Scandolo, S.; Crichton, W. A. Amorphous silica-like carbon dioxide. *Nature* **2006**, *441*, 857–860.

(10) Erements, M. I.; Gavriluk, A. G.; Trojan, I. A.; Dzivenko, D. A.; Boheler, R. Single-bonded cubic form of nitrogen. *Nat. Mater.* **2004**, *3*, 558–563.

(11) Chelazzi, D.; Ceppatelli, M.; Santoro, M.; Bini, R.; Schettino, V. High-pressure synthesis of crystalline polyethylene using optical catalysis. *Nat. Mater.* **2004**, *3*, 470–475.

(12) Iota, V.; Yoo, C. S.; Cynn, H. Quartzlike Carbon Dioxide: An Optically Nonlinear Extended Solid at High Pressures and Temperatures. *Science* **1999**, *283*, 1510–1513.

(13) Ceppatelli, M.; Santoro, M.; Bini, R.; Schettino, V. Fourier transform infrared study of the pressure and laser induced polymerization of solid acetylene. *J. Chem. Phys.* **2000**, *113*, 5991–6000.

(14) Aoki, K.; Usuba, S.; Yoshida, M.; Kakudate, Y.; Tanaka, K.; Fujiwara, S. Raman study of the solid-state polymerization of acetylene at high pressure. *J. Chem. Phys.* **1988**, *89*, 529–534.

(15) Sakashita, M.; Yamawaki, H.; Aoki, K. FT-IR Study of the Solid State Polymerization of Acetylene under Pressure. *J. Phys. Chem.* **1996**, *100*, 9943–9947.

(16) Chelazzi, C.; Ceppatelli, M.; Santoro, M.; Bini, R.; Schettino, V. Pressure-Induced Polymerization in Solid Ethylene. *J. Phys. Chem. B* **2005**, *109*, 21658–21663.

(17) Katz, A. I.; Schiferl, D.; Mills, R. L. New phases and chemical reactions in solid carbon monoxide under pressure. *J. Phys. Chem.* **1984**, *88*, 3176–3179.

(18) Mills, R. L.; Schiferl, D.; Katz, A. I.; Olinger, B. New phases and chemical reactions in solid CO under pressure. *J. Phys. (Paris), Colloq.* **1984**, *45*, C8-187–C8-190.

(19) Mills, R. L.; Olinger, B.; Cromer, D. T. Structures and phase diagrams of N<sub>2</sub> and CO to 13 GPa by x-ray diffraction. *J. Chem. Phys.* **1986**, *84*, 2837–2845.

(20) Lipp, M. J.; Evans, W. J.; Baer, B. J.; Yoo, C. S. High-energy-density extended CO solid. *Nat. Mater.* **2005**, *4*, 211–215.

(21) Evans, W. J.; Lipp, M. J.; Yoo, C. S.; Cynn, H.; Herberg, J. L.; Maxwell, R. S.; Nicol, M. F. Pressure-Induced Polymerization of Carbon Monoxide: Disproportionation and Synthesis of an Energetic Lactonic Polymer. *Chem. Mater.* **2006**, *18*, 2520–2531.

(22) Cromer, D. T.; Schiferl, D.; LeSar, R.; Mills, R. L. Room-temperature structure of carbon monoxide at 2.7 and 3.6 GPa. *Acta Crystallogr., Sect. C: Cryst. Struct. Commun.* **1983**, *39*, 1146–1150.

(23) Bernard, S.; Chiarotti, G. L.; Scandolo, S.; Tosatti, E. Decomposition and Polymerization of Solid Carbon Monoxide under Pressure. *Phys. Rev. Lett.* **1998**, *81*, 2092–2095.

(24) Rademacher, N.; Bayarjargal, L.; Morgenroth, W.; Winkler, B.; Ciezak-Jenkins, J.; Batyrev, I. G.; Milman. The Local Atomic Structures of Liquid CO at 3.6 GPa and Polymerized CO at 0 to 30 GPa from High-Pressure Pair Distribution Function Analysis. *V. Chem. - Eur. J.* **2014**, *20*, 11531–11539.

(25) Ceppatelli, M.; Serdyukov, A.; Bini, R.; Jodl, H. J. Pressure Induced Reactivity of Solid CO by FTIR Studies. *J. Phys. Chem. B* **2009**, *113*, 6652–6660.

(26) Santoro, M.; Gorelli, F. A.; Bini, R.; Haines, J.; van der Lee, A. High-pressure synthesis of a polyethylene/zeolite nano-composite material. *Nat. Commun.* **2013**, *4*, 1557.

(27) Scelta, D.; Ceppatelli, M.; Santoro, M.; Bini, R.; Gorelli, F. A.; Perucchi, A.; Mezouar, M.; van der Lee, A.; Haines, J. High Pressure Polymerization in a Confined Space: Conjugated Chain/Zeolite Nanocomposites. *Chem. Mater.* **2014**, *26*, 2249–2255.

(28) Santoro, M.; Dziubek, K.; Scelta, D.; Ceppatelli, M.; Gorelli, F. A.; Bini, R.; Thibaud, J.-M.; Di Renzo, F.; Cambon, O.; Rouquette, J.; Hermet, P.; van der Lee, A.; Haines, J. High Pressure Synthesis of All-Transoid Polycarbonyl  $[-(C=O)-]_n$  in a Zeolite. *Chem. Mater.* **2015**, *27*, 6486–6489.

(29) Olson, D. H.; Kokotailo, G. T.; Lawton, S. L.; Meier, W. M. Crystal structure and structure-related properties of ZSM-5. *J. Phys. Chem.* **1981**, *85*, 2238–2243.

(30) Hay, D. G.; Jaeger, H. Orthorhombic-monoclinic phase changes in ZSM-5 zeolite/silicalite. *J. Chem. Soc., Chem. Commun.* **1984**, 1433–1433.

(31) Sun, J.; Klug, D. D.; Pickard, J.; Needs, R. J. Controlling the Bonding and Band Gaps of Solid Carbon Monoxide with Pressure. *Phys. Rev. Lett.* **2011**, *106*, 145502.

(32) Di Renzo, F.; Remoué, F.; Massiani, P.; Fajula, F.; Figueras, F.; Des Courières, T. Crystallization kinetics of zeolite TON. *Zeolites* **1991**, *11*, 539–548.

(33) Mao, H. K.; Bell, P. M.; Shaner, J. V.; Steinberg, D. J. Specific volume measurements of Cu, Mo, Pd, and Ag and calibration of the ruby R<sub>1</sub> fluorescence pressure gauge from 0.06 to 1 Mbar. *J. Appl. Phys.* **1978**, *49*, 3276–3283.

(34) Haines, J.; Cambon, O.; Levelut, C.; Santoro, M.; Gorelli, F.; Garbarino, G. Deactivation of pressure-induced amorphization in silicalite SiO<sub>2</sub> by insertion of guest species. *J. Am. Chem. Soc.* **2010**, *132*, 8860–8861.

(35) Gorelli, F. A.; Ulivi, L.; Santoro, M.; Bini, R. The  $\epsilon$  Phase of Solid Oxygen: Evidence of an O<sub>4</sub> Molecule Lattice. *Phys. Rev. Lett.* **1999**, *83*, 4093–4096.

(36) Hammersley, A. P.; Svensson, S. O.; Hanfland, M.; Fitch, A. N.; Häusermann, D. Two Dimensional Detector Software: From Real Detector to Idealised Image Or Two-Theta Scan. *High Pressure Res.* **1996**, *14*, 235–248.

(37) Rodríguez-Carvajal, J. Recent developments of the program FULLPROF. *Comm. Powder Diffn. (IUCr) Newsllett.* **2001**, *26*, 12–19.

(38) Rodríguez-Carvajal, J.; Gonzalez-Platas, J. *GFOURIER Program 04.06*, A graphical tool for Fourier maps (x-ray & neutron data); 2007 (unpublished) <https://www.ill.eu/sites/fullprof/index.html>.

(39) Sanchez-Portal, D.; Ordejon, P.; Artacho, E.; Soler, J. M. Density-functional method for very large systems with LCAO basis sets. *Int. J. Quantum Chem.* **1997**, *65*, 453–461.

(40) Perdew, J. P.; Burke, K.; Ernzerhof, M. Generalized Gradient Approximation Made Simple. *Phys. Rev. Lett.* **1996**, *77*, 3865–3868.

(41) Ciabini, L.; Santoro, M.; Bini, R.; Schettino, V. High pressure reactivity of solid benzene probed by infrared spectroscopy. *J. Chem. Phys.* **2002**, *116*, 2928–2935.

(42) Marler, B. Silica-ZSM-22: synthesis and single crystal structure refinement. *Zeolites* **1987**, *7*, 393–397.